Gas Phase Chemistry in Gallium Nitride CVD: Theoretical Determination of the Arrhenius Parameters for the First Ga−C Bond Homolysis of Trimethylgallium

Rochus Schmid* and Daniel Basting†

Lehrstuhl für Anorganische Chemie II, Organometallics and Materials Chemistry, Ruhr-Universität Bochum, D-44780 Bochum, Germany, and Abt. Membranbiophysik & FK-NMR, Institut für Biophysikalische Chemie, J. W. Goethe Universität, Marie-Curie-Str. 9, D-60439 Frankfurt am Main, Germany

Received: October 12, 2004; In Final Form: January 5, 2005

Experimental evidence suggests that the energy of activation for the first homolytic Ga−C bond fission of $GaMe_3$ of $E_a = 249$ kJ/mol, measured by Jacko and Price in a hot-wall tube reactor, is affected by surface catalytic effects. In this contribution, the rate constant for this crucial step in the gas-phase pyrolysis of $GaMe_3$ has been calculated by variational transition state theory. By a basis set extrapolation on the MP2/cc-pVXZ level and a correlation correction from CCSD(T)/cc-pVDZ level, a theoretical "best estimate" for the bond energy of $\Delta H_{289K} = 327.2$ kJ/mol was derived. For the VTST calculation on the B3LYP/cc-pVDZ level, the energies were corrected to reproduce this bond energy. Partition functions of the transitional modes were approximated by a hindered rotor approximation to be valid along the whole reaction coordinate defined by the Ga−C bond length. On the basis of the canonical transition state theory, reaction rates were determined using the maxima of the free energy $\Delta G^{\ddagger}$. An Arrhenius-type rate law was fitted to these rate constants, yielding an apparent energy of activation of $E_a = 316.7$ kJ/mol. The preexponential factor $A = 3.13 \times 10^{16}$ 1/s is an order of magnitude larger than the experimental results because of a larger release of entropy at the transition state as compared to that of the unknown surface catalyzed mechanism.

1. Introduction

Wide-band gap semiconductors of group III/V elements are an important component of optoelectronic devices such as light-emitting diodes.[1] The major industrial route to gallium-nitride (GaN) thin films is via metal−organic chemical vapor deposition (MO-CVD), using trimethylgallium and a large excess of ammonia as precursors.[2] The industrial production of photoluminiscent films by the so-called high-pressure two-flow process has been pioneered by Nakamura and co-workers.[3,4] Nowadays, a simpler low-pressure process is routinely used in industrial production reactors. At elevated temperatures, the precursor decomposition leads to a complicated network of reactions both in the gas phase and on the surface. Despite the fact that this process has been optimized for film quality and yield, the underlying reaction mechanism is not yet fully understood. Experimental measurements allow the determination of overall activation energies via growth rates. However, valid thermodynamic or kinetic data for elementary steps, including reactive and unstable intermediates, is hard to achieve. In Scheme 1 two possible main routes to relevant growth intermediates are displayed in a very simplistic form.

One possibility is the pyrolysis of $GaMe_3$ by successive homolytic Ga−C bond fissions. Either GaMe or atomic Ga is then adsorbed on the surface, whereas NH_3 is directly activated on the hot surface. As an alternative, an ammonia adduct can be formed, which eliminates methane already at low temperatures, leading to cyclic oligomers ($n = 2$ or 3) of the gallium amide. This is essentially an in situ formation of a single molecule precursor. Presumably both reaction pathways are

SCHEME 1: Possible Growth Mechanisms in the $GaMe_3/NH_3$ System

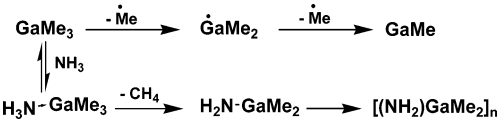

followed to some extent. It is, however, disputed as to which amount "GaN" species such as the gallium amides and its decomposition products are necessary and relevant for GaN film growth.[5] It should be noted that this is not only a scientific question. The design of CVD reactors relies on computational fluid dynamic simulations (CFD) to model physical transport in the gas phase.[6] Here, a valid chemical reaction mechanism for the growth process is of pivotal importance.

The important Arrhenius parameters for the first Ga−C bond homolysis, which is rate limiting for the $GaMe_3$ pyrolysis, were first determined by Jacko and Price (JP) in 1963 (first reaction on the top in Scheme 1).[7] A hot-wall tube reactor in connection with the toluene carrier method (to trap the formed radicals) was used to investigate gas-phase pyrolysis reactions and to deduce bond energies for quite a number of compounds. They found an energy of activation of 249 ± 23 kJ/mol[8] for the first Ga−C bond fission in $GaMe_3$. Early theoretical investigations by Oikawa et al. on the MP3 level of theory gave a higher value of 275 kJ/mol for the corresponding bond energy.[9] The authors reinterpreted the results by JP, omitting two data points, which gave a higher Arrhenius activation energy of 269 ± 18 kJ/mol. This value is very close to the results of a more recent mass spectroscopic investigation of Chen and Dapkus,[10] who measured an activation energy of 270 kJ/mol in inert nitrogen carrier gas.[11] However, high-level G2 calculations by Allendorf et al.

* Author to whom correspondence should be addressed: rochus.schmid@ruhr-uni-bochum.de.

† Institut für Biophysikalische Chemie, J. W. Goethe Universität.

10.1021/jp045343o CCC: $30.25
Published on Web 02/24/2005

gave a bond energy ΔH_{298K} of 321 kJ/mol,[12] which is substantially above all measured values. A similar discrepancy between experimentally determined bond energies by the method used by JP and theoretically calculated values was found also for other compounds, especially the higher homologue $InMe_3$. For this case, McDaniel et al. repeated the experimental measurement using a hot-wall tube reactor with a significantly improved measurement technology.[13] They found that only with a seasoned reactor were reproducible results for the reaction rates found. Cleaning of the reactor walls resulted in significantly slower reaction rates, which implies some unknown autocatalytic effects due to surface species or surface reactions. JP already mentioned in their paper on the $GaMe_3$ pyrolysis that the measured rate constants are "*... extremely sensitive to the nature of the surface in the reaction zone*".[7] In addition, experiments conducted by JP in a "packed vessel" with an increased surface-to-volume ratio showed an increase in the reaction rate. It must be concluded that the JP values do not correspond to the pure gas-phase pyrolysis of $GaMe_3$ or $InMe_3$. Despite these experimental and theoretical indications for a significantly larger activation energy of the first Ga−C homolysis, the original values published by JP are uncritically used in current reaction mechanisms for CFD modeling of GaN and GaAs deposition.[14−16]

It is important to note the difference between the apparent energy of activation, determined from experimental reaction rates, and bond energies calculated at thermodynamic equilibrium for infinitely separated fragments. For a true comparison with experiment (and for the use in CFD simulations), the actual temperature-dependent rate constants have to be calculated theoretically. Transition state theory (TST)[17] can be used to relate the unimolecular high-pressure limit rate constants k with the free energy of activation $\Delta G^{\ddagger}$ at a given temperature T according to

$$k = \sigma\tau\frac{k_B T}{h}\exp[-\Delta G^{\ddagger}/k_B T] \qquad (1)$$

Here σ is the reaction path degeneracy (which is 3 in the case of $GaMe_3$) and τ is the tunneling probability (which is assumed to be close to 1 in our case) and k_B and h are the Boltzmann and Planck constants, respectively. The assumption of a canonical behavior (high-pressure limit) is justified by the fact that JP did not observe any significant pressure dependence in their experiments (pressure range of 6−30 Torr).[18] The temperature-dependent $\Delta G^{\ddagger}$ is given as the maximum of ΔG along the reaction coordinate (rc). For a homolytic reaction, there is no energy maximum along the reaction path, and the position $rc^{\ddagger}$ for the maximum in $\Delta G^{\ddagger}$ is determined purely by entropic effects. As a result, $rc^{\ddagger}$ also is temperature dependent. The higher the temperature, the more pronounced are entropy effects and the earlier the TS will be situated along the rc. The energy at the transition state $\Delta E^{\ddagger}$ is lower than the value at infinite separation and its value is again temperature dependent, and the temperature-independent energy of activation E_a resulting from an Arrhenius or Eyring analysis is solely an apparent E_a not directly related to the bond energy (for infinitely separated fragments). The rather simple Gorin model, which to some extent accounts for the entropic effects, has been used by Smith and Patrick already in 1983 to extrapolate from the experimental kinetic data by JP to the thermodynamic bond energy ΔH_{298K}.[19] The resulting value for ΔH_{298K} of 261 kJ/mol is, however, only slightly higher than the measured E_a and does not account for the discrepancies between the measurement and the theoretically determined bond energies.

The experimental measurement of the pure gas-phase chemistry, excluding any surface effects, is hard to achieve. It is the intention of this contribution to calculate the rate constants purely on the basis of theoretical ab initio calculations free from any empiricism. Because of the barrier free radical process and the temperature dependence of $rc^{\ddagger}$, the so-called variational transition state theory (VTST) approach must be applied, searching for the maximum of ΔG along the reaction path.[20,21] Meanwhile, theoretical calculations are an important tool for the determination of CVD mechanisms.[22] In case of the $GaMe_3$/NH_3 precursor system, a wealth of thermodynamic information of "GaN" species as defined above has been determined theoretically by Timoshkin et al.; however, kinetics were neglected.[23−25] The group of Jensen et al. used DFT-type calculations to determine kinetic parameters via the calculation of nonradical transition states to derive reaction mechanisms for CFD modeling.[16,22,26] To our knowledge, the VTST-type treatment for a homolytic bond fission process within a CVD mechanism has not been performed yet. The theoretical determination of rate parameters for radical reactions is more established in the field of combustion chemistry as well as radical polymerization.[17,27] However, for example, in the case of a GaN single molecule precursor, we recently found a dominance of radical bond fission processes for the decomposition mechanism.[28] Thus, it is very important to establish a procedure to accurately determine necessary kinetic data for radical reactions for CVD precursors and intermediates.

We follow here roughly the procedure suggested by Lorant et al. for the determination of the homolytic C−C bond cleavage of ethane.[29] In the next section, the basic methodology of our theoretical method and computational details will be described. In the following sections, the calculated results are presented and discussed. After defining the reaction coordinate, we investigate the accuracy of the DFT-type calculations by correlated ab initio calculations, focusing on the thermodynamic reaction energy. Then, the approximation for the molecular partition function is discussed, followed by an analysis of the free-energy profiles along the reaction coordinate. Finally, the Arrhenius parameters derived from the free-energy maxima are discussed in comparison with the experimental values. The paper is finished with a concluding section, summarizing the results.

2. Computational Details

All calculations were performed on LINUX workstations using the Gaussian98 (release A.11) program suite.[30] For all VTST energy and frequency calculations, the density functional theory level with the spin polarized hybrid density functional B3LYP[31,32] together with the cc-pVDZ all electron basis set[33] for all elements was used. We have not used an effective core potential for gallium, since relativistic effects should be small, but core relaxation and core correlation effects are known to be crucial for Ga. Since our investigation focuses on the accurate calculation of especially low curvatures of the PES (low frequencies), we have used the "ultrafine" numerical integration grid (99 radial shells and 590 angular grid points) for the calculation of the exchange-correlation contributions. The Ga−C bond length was chosen as a reaction coordinate and was constrained to different values to sample the reaction coordinate. The "tight" convergence criterion was used for the geometry optimization of the other degrees of freedom because of our focus on low normal modes. An analytic calculation of the second derivatives of the energy with respect to the nuclei positions was performed for each constrained geometry. Because of the tight convergence criteria and the fine integration grid,

the unprojected Hessian matrix showed exactly six very small frequencies corresponding to the system's translational and rotational degrees of freedom. Despite these low values, we used the Hessian matrix with the translational and rotational contributions projected out for further analysis. It should be noted that because of the nonstationary nature of the geometries, the direction of the remaining gradient due to the Ga−C bond length constraint, which essentially represents the reaction coordinate, should also be projected out from the raw Hessian matrix. We found, however, that exactly one remaining normal mode resembling the *rc* (and having a negative curvature for most of the larger values of *rc*) has a very high projection on this gradient and is, therefore, naturally separated from the other degrees of freedom. Because of the breaking of spin symmetry that naturally occurs in a homolytic bond-breaking process within Kohn−Sham DFT and the sometimes small gaps between occupied and unoccupied orbitals along the reaction coordinate, it is difficult to converge the electronic degrees of freedom properly. We have adopted the simple strategy suggested by Lorant et al.,[29] starting out at large values of *rc* and moving slowly inward. The geometry and converged wave functions from the previous step were used as a starting point in each case. In critical cases, the wave function was analyzed via the stability analysis implemented into the Gaussian98 program package.[34] The calculated frequencies were used unscaled in the following calculation of the vibrational partition functions to avoid any empirical parameters in the calculation. Since we were mainly interested in the low transitional modes, any frequency scaling factor determined from a fit to experiment would not be reasonable.

To verify the accuracy of the B3LYP/cc-pVDZ level the reaction energy was calculated using the extended cc-pVTZ basis set. In addition, PUMP2 (unrestricted MP2 with spin contamination projected out) and UCCSD(T) single-point calculations at the B3LYP/cc-pVDZ geometries were performed using the default Gaussian98 settings for the number of the uncorrelated core states. For the PUMP2 calculations cc-pVTZ and cc-pVQZ also were used to extrapolate to the basis set limit. The basis set superposition error (BSSE) for these single-point calculations was corrected by the standard counterpoise technique.[35]

3. Results and Discussion

3.1. Reaction Coordinate and Geometries. The global minimum of the initial $GaMe_3$ molecule on the B3LYP/cc-pVDZ level has C_3h symmetry, whereas the final radical $GaMe_2$ is C_2v symmetric. Thus, the two remaining methyl groups are mirror symmetric in the final product, which is not the case initially. For the VTST analysis, it is important to keep the symmetry along the reaction coordinate. In addition, the assignment of vibrational frequencies for the determination of the partition functions described in the next paragraph was found to be much easier for symmetry-related spectator methyl groups. We, therefore, constrained the system to a C_s symmetry with mirror-symmetric methyl groups throughout the reaction (see Figure 1). This allows for a C_2v symmetric final state, but the initial optimized structure in C_s symmetry (Figure 1a) shows one imaginary frequency corresponding to methyl rotations (ν = i26 1/cm). All methyl rotations in this system are basically free rotors, especially for high temperatures, and are treated as such in the thermodynamic analysis. As an example, the energy difference between the C_{3h} symmetric global minimum and the C_s symmetric initial geometry is only 0.1 kJ/mol. This is negligible in light of the approximations made for the determination of the entropic contributions to the free energy *G*. As a consequence, we accepted the appearance of imaginary frequencies for these low-frequency rotational modes. In this case, the system is on the maximum of a very flat periodic potential for the methyl rotation. We simply used the corresponding real frequency for further analysis, which only means a slightly too high total energy but has no consequences for the entropic contributions.

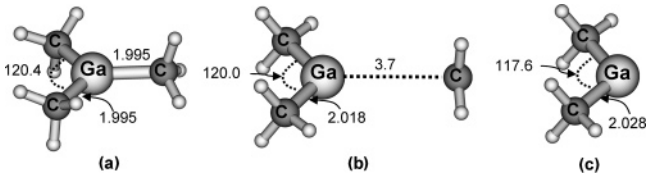

Figure 1. Example geometries used for the VTST analysis: (a) initial C_s symmetric structure, (b) intermediate structure for Ga−C constrained to 3.7 Å, and (c) final minimum structure for the $GaMe_2$ radical (distances in Å and angles in deg).

TABLE 1: Reaction Energies for the First Ga−C Bond Homolysis of $GaMe_3$ Using the B3LYP/cc-pVDZ Optimized Geometries (see Figure 1)

	ΔE^a [kJ/mol]	$\Delta E^{BSSE\ a,b}$ [kJ/mol]
B3LYP/cc-pVDZ	303.7	298.7
B3LYP/cc-pVTZ[c]	303.4	301.3
PUMP2/cc-pVDZ	322.6	304.4
PUMP2/cc-pVTZ	347.3	329.0
PUMP2/cc-pVQZ	352.0	339.0
PUMP2/extrap.[d]	353.1	345.7
UCCSD(T)/cc-pVDZ	317.5	297.6

[a] Pure reaction energies without ZPE correction. [b] BSSE correction included. [c] Geometries on the B3LYP/cc-pVTZ level of theory. [d] Extrapolation to the basis set limit according to the procedure described in the text.

For the unconstrained C_s symmetric initial molecule, the equilibrium bond length is 1.995 Å for the Ga−C bond in the symmetry plane. This interatomic distance was chosen as the reaction coordinate and was in turn constrained to values between 1.9 Å up to 5.0 Å in intervals of about 0.1 Å (0.2 Å above a *rc* value of 4.1 Å). In addition, in critical areas of the reaction coordinate, a finer spacing of only 0.05 Å was chosen. Another reference calculation was performed at 10 Å to investigate the asymptotic behavior. All other degrees of freedom except the reaction coordinate were optimized (maintaining C_s symmetry). At a Ga−C distance of 3.2 Å, the spin symmetry starts to get broken and the spin polarized system becomes lower in energy. Around 3.7 Å (Figure 1b) the leaving methyl group is already nearly planar. The Ga−C bond length in the remaining fragment slightly increases, whereas the C−Ga−C angle diminishes. This trend continues further to the free radical (Figure 1c). The structural changes in the $GaMe_2$ fragment are, however, only modest.

3.2. Reaction Energies. The reaction energies (starting from the C_s symmetric reactant as shown in Figure 1) for the Ga−C bond fission were used to benchmark the accuracy of our DFT level used for the VTST calculation. All calculated energies with and without BSSE correction are given in Table 1. In the case of the B3LYP/cc-pVTZ calculations, the geometries were also fully optimized on this level of theory. Obviously, the double-ζ quality basis set is already well converged, since both BSSE and the difference of the triple-ζ basis set values are very small. A part of the BSSE is actually compensated by basis set incompleteness. Thus, the cc-pVDZ is absolutely sufficient for the DFT calculations. In our search for a high-level ab initio reference value, we followed the strategy used by Pelekh and

Carr in their investigation of the adduct formation of $GaMe_3$ and NH_3.[36] As expected, the correlated ab initio results are much more sensitive to the basis set size than are the DFT values. The PUMP2 reaction energies are all well above the DFT results and grow significantly with increasing basis set size. This explains why both Oikawa et al. (294 kJ/mol on MP3 level)[9] and Bock et al. (309 and 314 kJ/mol on QCISD and MP4SDQ level, respectively)[37,38] found slightly lower reaction energies because of the smaller basis sets used in these earlier investigations. Even at the PUMP2/cc-pVQZ level, a substantial BSSE of 13.0 kJ/mol is observed. The difference between PUMP2/cc-pVDZ and UCCSD(T)/cc-pVDZ is, on the other hand, rather small. The basis set limit $\Delta E(\infty)$ for the PUMP2 calculations was extrapolated by fitting the results $\Delta E(n)$ with $\Delta E(n) = \Delta E(\infty) + \alpha \exp(-\beta n)$ for $n = 2$, 3, or 4 (cardinal number of the basis set).[39,40] By correcting the extrapolated PUMP2 value (including BSSE corrections) of 345.7 kJ/mol by the difference between UCCSD(T) and PUMP2, we arrive at our best theoretical estimate for the electronic reaction energy of 338.9 kJ/mol. Using the B3LYP/cc-pVDZ calculated frequencies for the ZPE and finite temperature corrections, a reaction enthalpy of $\Delta H_{298K} = 327.2$ kJ/mol results. This is very close to the value of $\Delta H_{298K} = 320.7$ kJ/mol calculated on the G2 level by Allendorf et al. and corroborates their findings.[12] The deviation between the basis set extrapolated PUMP2 values with and without BSSE correction of 7.4 kJ/mol indicates that the extrapolation was not complete and even larger basis sets would have to be included. However, this can be used as an estimate for the systematic error for the bond energy of about ±10 kJ/mol. This is also consistent with the deviation from the G2 value, which is based on a completely different extrapolation scheme.[41] For the further VTST analysis we have, therefore, applied a two-level approach as already proposed by others.[27] All geometries and vibrational frequencies were calculated on the B3LYP/cc-pVDZ level of theory. The calculated DFT energies along the reaction path were scaled by a factor of 1.1159 = 338.9/303.7 to match the estimated reaction energy of 338.9 kJ/mol at infinite separation. In the further discussion, we will refer to this corrected electronic energy as ΔE_{elec}, and the corresponding zero-point energy-corrected energy is termed ΔE_{0K}.

3.3. Partition Functions. For the variational transition state theory (VTST) approach, the maximum of $\Delta G(rc)$ along *rc* must be determined. The relative free energy is given as $\Delta G(rc) = G_{react} - G(rc)$, where G_{react} is the free energy of the reactant molecule $GaMe_3$ (including contributions from all 3N-6 internal degrees of freedom with N the number of atoms) and $G(rc)$ the corresponding free energy of the system at the given value of *rc* (including only 3N-7 internal contributions without the *rc*). The value of *G* is determined from the partition function *q* via

$$G = -RT \ln(q) \tag{2}$$

with the total partition function $q = q_{elec}q_{trans}q_{rot}q_{int}$. For the nondegenerate ground state and without thermal occupation of excited states, the electronic partition function is given by $q_{elec} = \exp(-\Delta E_{elec}/RT)$.[42] The translational partition function q_{trans} is constant, and the rotational partition function q_{rot} of the total system can be approximated by the static rotor partition function.[43] The major source of entropy released during the reaction stems from the conversion of internal vibrational degrees of freedom into rotations of the formed fragments, usually referred to as "transitional modes". Thus, the key point of the calculation is the accurate modeling of the increase in q_{int} along the reaction coordinate.

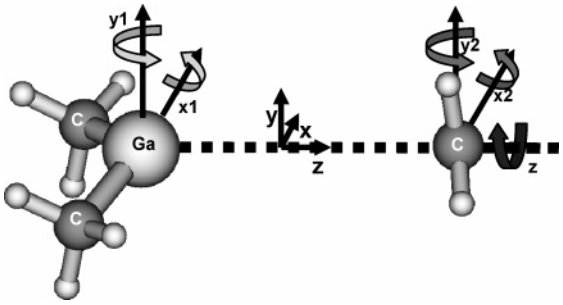

Figure 2. Definition of axes and nomenclature of transitional modes.

During the reaction, two radical fragments are formed out of the initial molecule, and six internal modes are converted. One of these modes is the reaction coordinate itself, which can be discarded in the determination of $G^{\ddagger}$ since it is converted to the k_BT/h prefactor in the TST. The assignment of the other five "transitional modes" is shown in Figure 2. The reaction coordinate defines the *z*-axis, and the *x*-axis is taken to be in the C−Ga−C plane. The rotation around the Ga−C bond (fragments rotating against each other around the reaction coordinate) is labeled **z**. The two C−Ga−C bending modes (in-plane and out-of-plane) are converted into the two rotational motions of the gallium fragment $GaMe_2$ (fragment 1) around the *x*- and *y*-axis. They are labeled **x1** and **y1**, respectively. The two methyl rocking modes of the displaced methyl group (fragment 2) are transformed into the corresponding rotations **x2** and **y2**. It is helpful to visualize how the translational and rotational degrees of freedom of the fragments are related to those of the initial $GaMe_3$ molecule. The six translations of the fragments correspond to the three translational degrees of freedom of $GaMe_3$ plus three relative translations. The latter are the reaction coordinate (relative motion along *z*) and the two global rotations of the total molecule around *x*- and *y*-axis, denoted by **rx** and **ry**. The six-fragment rotational degrees of freedom correspond to the five transitional modes **z**, **x1**, **y1**, **x2**, and **y2** plus the global *z*-rotation **rz**. Because of the elongation of the Ga−C bond, the moments of inertia, and thus, the partition functions for **rx** and **ry** change significantly. On the other hand, the partition functions for both **rz** and the transitional mode **z** do not change very much along the *rc*. As a consequence, the entropic contributions from **rx**, **ry**, and the transitional modes **x1**, **y1**, **x2**, and **y2** are the main source for the released entropy along the reaction. They are crucial for the accurate determination of $\Delta G^{\ddagger}$.

The three moments of inertia of the total system (**rx**, **ry**, **rz**) were determined via standard algorithms, and the rotational partition function q_{rot} was then calculated using the static rotor approximation. The partition functions for the majority of internal degrees of freedom were determined by the well-known harmonic oscillator, approximated using the calculated vibrational frequencies ν according to[44]

$$q_{ho} = \frac{\exp(-\Theta/2T)}{1 - \exp(-\Theta/T)}; \quad \Theta = \frac{h\nu}{k_B} \tag{3}$$

For very low frequencies corresponding to nearly free internal rotations, q_{ho} becomes, however, unphysically large and must be replaced by some hindered rotor approximation that gives the free rotor partition function q_{fr} for a zero frequency ν. We used the interpolation formula suggested by Truhlar for the hindered rotor partition function q_{hr} given as

$$q_{hr} = q_{ho} \tanh((\Theta/T)q_{fr}), \tag{4}$$

which was found to yield a satisfactory accuracy when compared with much more involved procedures.[45] From eq 4, it is obvious that solely the value of the free rotor partition function q_{fr} of the corresponding motion in addition to ν is needed for the determination of q_{hr}. For decreasing ν, the value q_{hr} starts to deviate from q_{ho} and smoothly reaches q_{fr} in the limit. Since the five transitional modes change from vibrations to rotations, the vibrational frequencies ν eventually become zero, and the hindered rotor partition function has to be applied here. In addition, the symmetric (**ms**) and anti symmetric (**ma**) methyl rotations of the two methyl groups in fragment 1 were also treated with the hindered rotor approximation. It should be noted that the hindered rotor approximation also alleviates the problem of large changes of the ΔG values because of numerical instabilities for the low vibrational frequencies that can lead to variations of 5−10 wavenumbers from step to step.

The major remaining problem was the determination of q_{fr} since none of the normal modes corresponds to a pure rotational motion of two fragments around a common axis. The approximate procedure to achieve this is explained in the following. First, the calculated normal modes were visually inspected[46] and the *rc*, the five transitional modes, and the methyl rotations (**ms** and **ma**) were assigned accordingly (see definitions in Figure 2). With one exception (due to a coupling of **ms** and **x1**, which is explained later on), this was possible without any ambiguities. Second, the corresponding rotational motions were defined by grouping the atoms into two fragments rotating against each other around a common axis. For the transitional modes, the fragments were always chosen to be the fragments 1 ($GaMe_2$) and 2 (Me). For **z**, the axis of rotation was taken to be parallel to the *z*-axis through the center of gravity of the total system. For **x1**/**y1** and **x2**/**y2**, the axis of rotation was defined to be parallel to the *x*- or *y*-axis going through the center of gravity of fragment 1 and 2, respectively. The moment of inertia I_1 and I_2 of the two fragments were combined to the total reduced moment of inertia $I = I_1I_2/(I_1 + I_2)$. The free rotor partition function is then calculated by (where σ_r is the symmetry number of the rotation)

$$q_{fr} = \frac{2\pi\sqrt{2\pi k_B T I}}{h\sigma_r} \tag{5}$$

As an example, in **x1** can be seen a rotation of the $GaMe_2$ fragment around its center of gravity, compensated by a rotation of the methyl group in the opposite direction, leading to a zero net rotational momentum. For small Ga−C distances, both I_1 and I_2 of the two fragments are similar, and the corresponding motion closely resembles the out-of-plane C−Ga−C bending motion. For very large Ga−C distances (end of the reaction), however, I_2 is becoming very large and $I \approx I_1$, which corresponds to a pure rotation of fragment 1. Thus, these motions and their moments of inertia are correct in the limit for the separated fragments. For intermediate values, they closely resemble the corresponding vibrational modes, which are no true rotations themselves. The exact value of q_{fr} is of importance only for low frequencies and large *rc*. Together with the hindered rotor partition function (eq 4), this procedure gives a consistent approximation for the partition function of the transitional modes, starting from the vibrational motion in the beginning of the reaction all the way to the final state of independently rotating radical fragments. Only the (assigned) vibrational frequencies and the geometry are necessary as input.

The two methyl rotations are also treated by the hindered rotor approximation. The reduced moment of inertia I_{Me} is identical for both methyl groups because of symmetry. The moments of inertia for the symmetric (**ms**) and asymmetric (**ma**) combinations were calculated according to the formulas for "Me−X−Me" fragments given in Smith[47] (see Supporting Information for details). The hindered rotor partition function for these modes was calculated with eq 5 and eq 4 exactly as for the transitional modes.

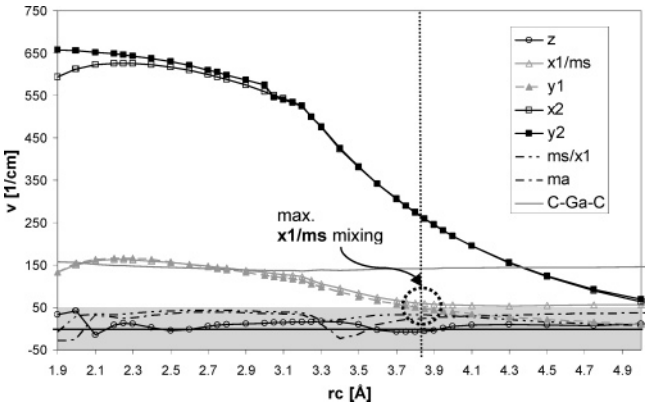

Figure 3. Calculated vibrational frequencies of the transitional modes along the reaction coordinate. The frequencies of the methyl rotations and the C−Ga−C bending mode of the formed $GaMe_2$ fragment are included. The shaded area represents the frequency range for free rotation of the methyl groups.

An additional problem was the coupling of **ms** and **x1**. Initially, **x1** has a much larger frequency than **ms** and is well separated. However, during the reaction, the frequency of **x1** diminishes, and at some point ($rc \approx 3.8$ Å), the two normal modes are an additive and subtractive mixture of the two motions, unmixing again for larger values of *rc* in a reversed way. This does not pose any problems for the harmonic partition function. However, because of the difference in the values of q_{fr}, a sudden swapping of the assignment of **x1** and **ms** leads to a discontinuity in q_{hr}. The resulting kink in the $G^{\ddagger}$ curve is only about 2 kJ/mol high but leads to difficulties in the determination of the exact maximum. Thus, we interpolated the q_{fr} used in eq 4 for both modes in a consistent fashion according to

$$q_{fr}^1 = (q_{fr}^{ms}/q_{fr}^{x1})^{\lambda} q_{fr}^{x1}; \quad q_{fr}^2 = (q_{fr}^{x1}/q_{fr}^{ms})^{\lambda} q_{fr}^{ms} \tag{6}$$

The parameter λ changes continuously from 0 to 1, converting q_{fr}^1 from q_{fr}^{x1} to q_{fr}^{ms} and vice versa. For all values of λ, the product $q_{fr}^1 q_{fr}^2$ is equal to $q_{fr}^{x1} q_{fr}^{ms}$. The value of λ was determined as the averaged relative contributions of the **x1** and **ms** (internal coordinate) motions to the two normal modes. A so-called "potential energy distribution" analysis[48] was performed for each geometry to derive these contributions. (Further details about this analysis and the determination of the λ values is given in the Supporting Information.) This procedure resulted in smooth $\Delta G(rc)$ curves without altering their values by more than 1 kJ/mol.

3.4. Free Energies of Activation. The major gain in entropy during the reaction originates from the rotational degrees of freedom **rx** and **ry** and the transitional modes, determined mainly by the vibrational frequencies. In Figure 3, these frequencies are plotted with respect to the reaction coordinate. We observed a slight discontinuity in the slope of these curves at $rc = 3.2$ Å because of the onset of spin polarization, which vanishes if the spin restricted systems higher in energy would be used. This does not, however, affect the evaluation of $\Delta G^{\ddagger}$ because the maximum in ΔG is always found at *rc* values larger than 3.2 Å, even at temperatures as high as 1600 K. The

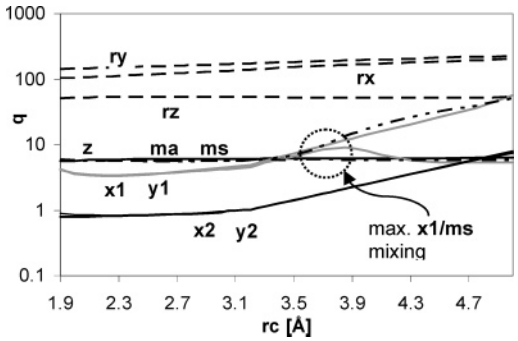

Figure 4. Partition functions of the transitional modes (**x1**, **y1**, **x2**, **y2**, **z**; black and gray solid lines), spectator methyl rotations (**ma**, **ms**; dash dotted lines) and the global rotational degrees of freedom (**rx**, **ry**, **rz**; dashed lines) in a logarithmic scale for $T = 800$ K.

transitional modes **x1** and **y1** represent initially C−Ga−C bending modes with frequencies around 150 1/cm. During the reaction, they decrease to values close to zero already at $rc = 5.0$ Å, converting into free rotations of the $GaMe_2$ fragment (Note the conversion of **x1** into **ms** for $rc > 3.9$ Å). In contrast to that, the third C−Ga−C bending mode of the $GaMe_2$ fragment, shown for comparison, does not change significantly. Even larger is the drop of the methyl rocking modes **x2** and **y2** upon conversion into the methyl radical rotations. The frequencies of the spectator methyl rotations **ms** and **ma** as well as **z**, on the other hand, always remain in the area below 50 1/cm (shaded area in Figure 3), corresponding to a nearly free internal rotation.

From these vibrational frequencies and the corresponding molecular geometries, the partition functions for all degrees of freedom have been calculated as described in the previous section. The partition functions for the transitional modes and the molecular rotation at a temperature of $T = 800$ K are shown in Figure 4 in a logarithmic scale to analyze the individual contributions for the changes in $\Delta G(rc)$ along the reaction coordinate. As expected, $\ln(q_{rot})$ for **rx** and **ry** increases almost linearly because of the increasing separation of the fragments, whereas the contribution form **rz** remains constant. A larger increase in $\ln(q)$ is observed for the internal degrees of freedom **x1**, **y1**, **x2**, and **y2** when the Ga−C bond starts to be broken. Because of the mixing of **x1** and **ms**, these two curves "exchange" above $rc = 3.9$ Å. Since the partition function of the methyl rotation is basically constant, the product of q for **x1** and **ms** would show a similar behavior as **y1**. Despite the difference in the absolute value, the $\ln(q)$ of the transitional modes for both fragments have a similar slope and, therefore, result in a similar entropy increase during the reaction, which is larger than the contribution from the overall molecular rotations.

On the basis of the total partition function q, $\Delta G(rc)$ is calculated using eq 2 for various temperatures. In Figure 5, the absolute zero potential energy E_{0K} relative to the initial $GaMe_3$ molecule (in C_s symmetry) is shown as the thick line converging to a value of 320.9 kJ/mol. In addition, the ΔG curves for selected temperatures in the range from 400 to 1400 K relevant for CVD applications are shown.[49] The value of $rc^{\ddagger}$ reduces with increasing temperatures from $rc^{\ddagger} = 4.31$ Å at 400 K to $rc^{\ddagger} = 3.46$ Å at 1600 K, resulting in a strong temperature dependence of $\Delta E^{\ddagger}$. In accordance with this, the maximum $\Delta G^{\ddagger}$ also decreases for higher temperatures. Using eq 1, the temperature-dependent VTST rate constants $k(T)$ have been calculated. The calculated numeric results used for the following Arrhenius plot are summarized in Table 2.

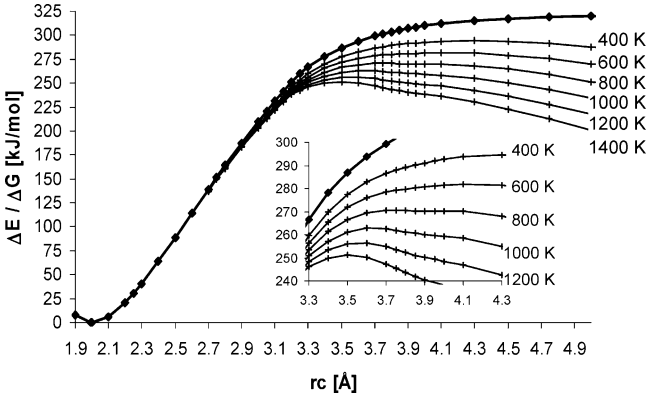

Figure 5. Relative zero temperature energy ΔE_{0K} (thick line) and $\Delta G(rc)$ for various temperatures.

TABLE 2: Transition State Parameters and Calculated VTST Rate Constants

T [K]	$rc^{\ddagger}$ [Å]	$\Delta E^{\ddagger}$ [kJ/mol]	$\Delta G^{\ddagger}$ [kJ/mol]	$k(T)$ [1/s]
400	4.31	315.3	294.5	8.86×10^{-26}
450	4.26	314.6	291.2	4.44×10^{-21}
500	4.21	313.9	288.1	2.54×10^{-17}
600	4.09	311.8	281.9	1.09×10^{-11}
700	4.05	311.1	276.1	1.10×10^{-7}
800	3.75	301.8	270.5	1.09×10^{-4}
900	3.71	299.9	266.4	1.94×10^{-2}
1000	3.64	296.1	262.9	1.17×10^{0}
1100	3.60	293.9	259.5	$3.27 \times 10^{+1}$
1200	3.56	291.5	256.5	$5.13 \times 10^{+2}$
1300	3.53	289.6	253.9	$5.13 \times 10^{+3}$
1400	3.51	287.7	251.3	$3.67 \times 10^{+4}$
1500	3.48	285.7	249.0	$2.00 \times 10^{+5}$
1600	3.46	283.7	246.9	$8.69 \times 10^{+5}$

The rate constants given in Table 2 have been used to determine the parameters for the Arrhenius-type rate law $k = A \exp(-E_a/RT)$ via a linear regression of $\ln(k)$ over the inverse temperature shown in Figure 6. Since the Arrhenius rate law is not exactly valid, the result depends on the temperature range used for the analysis. In contrast to the rather small range used in the experimental investigations (see scattered data points in Figure 6; open triangles), we have included the full temperature range relevant in CVD applications. The $\ln(k)$ values can be fit very well with a linear curve with a modest deviation at higher temperatures. For comparison, the experimentally determined Arrhenius curve from JP ($E_a = 249$ kJ/mol; $A = 3.16 \times 10^{15}$ 1/s; dashed line) is also shown.[7] The apparent activation energy

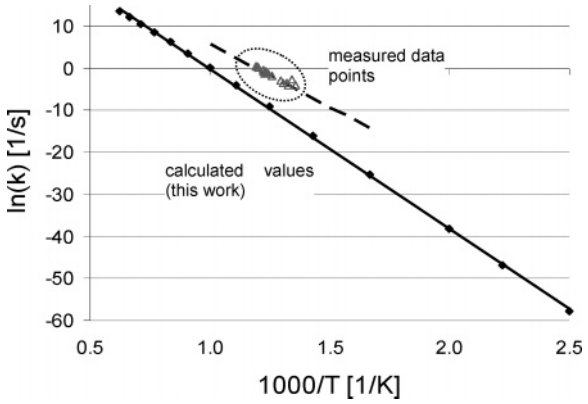

Figure 6. Logarithmic rate constants given in Table 2 with respect to the inverse temperature (solid line is the linear regression). The open triangles are the measured values by JP ("unpacked vessel" runs from Table 1B[7]) and the dashed line is the corresponding Arrhenius fit given by JP.

calculated from our results is $E_a = 316.7$ kJ/mol, and the preexponential factor is $A = 3.13 \times 10^{16}$. Thus, our results predict a significantly lower reaction rate for the pure gas-phase reaction as compared to the surface-catalyzed values measured by JP. On the other hand, the calculated preexponential factor is an order of magnitude larger, which can be explained by a larger amount of entropy released at the TS for a unimolecular decomposition in comparison to a reaction on a surface site. In contrast to the error margins for the potential energy, it is very difficult to estimate the systematic error because of inaccuracies in the partition functions. However, the influence is much larger on the preexponential factor A than on the energy of activation. From our experience with different levels of approximation for the partition functions for the transitional modes, we estimate the total inaccuracy in E_a to be about ±15 kJ/mol. It should be noted that the similarity between E_a and the zero-point reaction energy at infinite separation is a coincidence resulting from the complex dependence of both $\Delta E^{\ddagger}$ and $\Delta S^{\ddagger}$ on the temperature. Preliminary calculations for a similar homolytic bond fission for a Ga−Et bond revealed higher entropic contributions because of the higher mass of the formed ethyl radical compared to that of methyl.[50] In this case, the larger reaction rates manifested in a substantial lowering of the apparent activation energy compared to the thermodynamic reaction energy.

At this point, we would like to note that Oikawa et al. already have undertaken a VTST-type treatment in their early theoretical investigation.[9] However, in their approach, the vibrational frequencies of the transitional modes were not calculated all along the transition state but modeled by an analytical function including an empiric parameter. This parameter was fitted to reproduce the measured rate constant of about 0.5 1/s at 817 K. For this temperature, $rc^{\ddagger}$ was found to be 4.20 Å, which is significantly larger than our value of 3.75 Å at 800 K (see Table 2). Thus, the low reaction energy (because of a small basis set used for the MP3 calculation) and the loose TS erroneously reproduced the higher rate constants measured by JP. Because of the empirical fit involved, this has, however, no predictive capability. In a very recent theoretical study, Sengupta investigated the methane elimination from the $GaMe_3$ ammonia adduct (see Scheme 1), demonstrating that this is a chemically activated reaction.[5] In this context, he also investigated the first Ga−C bond fission of $GaMe_3$ using DFT (B3LYP functional). The bond energies are very similar to the ones we calculated on the DFT level. However, for the determination of $\Delta G^{\ddagger}$, the critical value of $rc^{\ddagger}$ was empirically chosen to be 2.8 times the Ga−C equilibrium distance. This results in an $rc^{\ddagger}$ of about 5.6 Å, which is far too loose and leads to a significant underestimation of $\Delta G^{\ddagger}$ (see Figure 5). The resulting reaction rates are thus much higher and again erroneously reproduced the JP experimental data.

4. Conclusion

Experimental findings indicate that the rate constants for the first Ga−C bond homolysis of $GaMe_3$ measured in hot-wall tube reactors are too high because of surface catalytic effects.[13] This is also supported by various theoretical calculations of the thermodynamic bond energy, which is found to be much higher than the experimental estimate.[12] In this contribution, we calculated the Arrhenius parameters for this important reaction step purely from first principles.

On the ab initio MP2 level using the cc-pVXZ series of basis sets (X = D, T, and Q, including BSSE correction) together with a basis set extrapolation and a correction for the difference between CCSD(T) and MP2 level on the cc-pVDZ basis set, we determined our best estimate for the electronic reaction energy to be $\Delta E_{elec} = 338.9$ kJ/mol. This value is nearly 10% larger than the corresponding energy on B3LYP/cc-pVDZ level ($\Delta E_{DFT} = 303.7$ kJ/mol). On the ab initio level, the basis set convergence is rather slow. The reaction energy increases with the basis set size, which explains the lower values found in previous investigations with smaller basis sets. With the zero-point energy and enthalpy corrections resulting from the B3LYP frequency analysis, a bond energy of $\Delta H_{298K} = 327.2$ kJ/mol is found, which is only slightly larger than the 320.9 kJ/mol calculated on the G2 level by Allendorf et al.[12]

On the basis of this calculated reaction energy, we have corrected the DFT energies on B3LYP level to locate the maximum of the relative free energy $\Delta G^{\ddagger}$ in a VTST-type approach. Geometries and frequencies were calculated on the B3LYP level along the reaction coordinate defined as the Ga−C distance. The partition functions were calculated within the standard approximations. For the freely rotating methyl groups and the transitional modes, which are converted to fragment rotations during the reaction, a hindered rotor approximation was employed. As expected for a barrier-free reaction, not only $\Delta G^{\ddagger}$ but also the location of the TS ($rc^{\ddagger}$) and $\Delta E^{\ddagger}$ are largely temperature dependent. Despite the complex temperature dependence of the canonical rate constant on the various thermodynamic properties, they could be fitted well by a simple Arrhenius-type rate law over a wide temperature range from 400 to 1600 K. The apparent energy of activation was calculated to be $E_a = 316.7$ kJ/mol with a preexponential factor of $A = 3.13 \times 10^{16}$ 1/s. We estimate the systematic error in the energy of activation to be about ±15 kJ/mol. Thus, neither the deviation from the value of 249 ± 23 kJ/mol measured by JP nor from the result of Chen and Dapkus of 270 kJ/mol can be attributed to inaccuracies of measurement or theory. As a consequence, the assumption that the measured depletion of $GaMe_3$ or the formation of methyl radicals or CH_4 is solely due to a homogeneous unimolecular Ga−C bond-breaking process does not hold. Instead, the experimental results from the hot-wall tube reactors represent an integral result of a much more complex homogeneous and heterogeneous reaction system, which was discussed in more detail for the similar case of $InMe_3$.[13]

Despite the approximations made especially for the calculation of the partition functions, we consider our calculated rate parameters as the currently best theoretical estimate for the pure unimolecular gas-phase reaction, which should be used in CFD modeling of CVD processes involving $GaMe_3$. In principle, besides increasing the theoretical level or using more sophisticated approximations for the internal rotor partition functions, molecular dynamics or Monte Carlo-type approaches could be employed to sample the phase space; however, this means a substantially larger computational effort. It would be very desirable if this crucial reaction could be experimentally reinvestigated, completely excluding any surface reactions, to yield an accurate measured value for the rate constants for the pure gas-phase pyrolysis. It appears, however, to be difficult to conduct such an experiment. On the other hand, a theoretical model, including surface reactions explaining the lower rate constants found in the hot-wall reactor experiment, would also corroborate our interpretation. It should be noted that this more complex pyrolysis mechanism of $GaMe_3$ is presumably active also in the CVD process of GaN itself. We are currently underway to apply the methodology worked out in this contribution to other gas-phase reactions in the classical $GaMe_3$

ammonia precursor system as well as the single-molecule precursor investigated previously.[28]

Acknowledgment. We thank Roland A. Fischer and Wolfgang A. Herrmann for their support of our research. We are very grateful to Mark D. Allendorf for helpful discussions in the course of this project. Maxim Tafipolsky is acknowledged for help with the potential energy distribution program. The "Deutsche Forschungs Gemeinschaft" financially supported this work within the SPP-1119 research program. The "Alfried Krupp von Bohlen und Halbach Stiftung" is thanked for generous donation of the LINUX computer cluster used in this work.

Supporting Information Available: A listing of the computed geometries and harmonic frequencies of $GaMe_3$ used for the VTST analysis, the moments of inertia for the calculation of the partition functions, and the $\Delta G(rc)$ for all investigated temperatures are given; in addition, details on the calculation of the partition functions are elaborated (see Section 3.3). This material is available free of charge via the Internet at http://pubs.acs.org.

References and Notes

(1) Nakamura, S.; Fasol, G. *The Blue Laser Diode: GaN Based Light Emitters and Lasers*; Springer-Verlag Telos: New York, 1997.

(2) Stringfellow, G. B. *Organometallic Vapor-Phase Epitaxy: Theory and Practice*, 2nd ed.; Academic Press: New York, 1999.

(3) Nakamura, S.; Harada, Y.; Seno, M. *Appl. Phys. Lett.* **1991**, *58*, 2021.

(4) Nakamura, S.; Sakai, S. In *Jpn. Kokai Tokkyo Koho*; Nichia KagakuKogyo K. K.: Tokyo, 1991, p 8.

(5) Sengupta, D. *J. Phys. Chem. B* **2003**, *107*, 291.

(6) Jensen, K. F. *Proc.—Electrochem. Soc.* **1984**, *84−6*, 3.

(7) Jacko, M. G.; Price, S. J. W. *Can. J. Chem.* **1963**, *41*, 1560.

(8) The error margins are taken from Oikawa et al. (ref 9).

(9) Oikawa, S.; Tsuda, M.; Morishita, M.; Mashita, M.; Kuniya, Y. *J. Cryst. Growth* **1988**, *91*, 471.

(10) Chen, Q.; Dapkus, P. D. *J. Electrochem. Soc.* **1991**, *138*, 2821.

(11) Unfortunately, no error estimates of the energies of activation are given in ref 10.

(12) Allendorf, M. D.; Melius, C. F.; Bauschlicher, C. W., Jr. *J. Phys. IV* **1999**, *9*, 23.

(13) McDaniel, A. H.; Allendorf, M. D. *Chem. Mater.* **2000**, *12*, 450.

(14) Safvi, S. A.; Redwing, J. M.; Tischler, M. A.; Kuech, T. F. *J. Electrochem. Soc.* **1997**, *144*, 1789.

(15) Theodoropoulos, C.; Mountziaris, T. J.; Moffat, H. K.; Han, J. *J. Cryst. Growth* **2000**, *217*, 65.

(16) Mihopoulos, T. G.; Gupta, V.; Jensen, K. F. *J. Cryst. Growth* **1998**, *195*, 733.

(17) Gilbert, R. G.; Smith, S. C. *Theory of Unimolecular and Recombination Reactions*; Blackwell Science: Cambridge, MA, 1990.

(18) It has been pointed out by a reviewer that, if unimolecular falloff conditions would be present, the discrepancy between experimental and theoretical results would be even larger.

(19) Smith, G. P.; Patrick, R. *Int. J. Chem. Kinet.* **1983**, *15*, 167.

(20) Truhlar, D. G.; Garrett, B. C.; Klippenstein, S. J. *J. Phys. Chem.* **1996**, *100*, 12771.

(21) Gordon, M. S.; Truhlar, D. G. *Science* **1990**, *249*, 491.

(22) Simka, H.; Willis, B. G.; Lengyel, I.; Jensen, K. F. *Prog. Cryst. Growth Charact. Mater.* **1998**, *35*, 117.

(23) Timoshkin, A. Y.; Bettinger, H.; Schaefer, H. F. *J. Cryst. Growth* **2001**, *222*, 170.

(24) Timoshkin, A. Y.; Bettinger, H. F.; Schaefer, H. F., III. *J. Phys. Chem. A* **2001**, *105*, 3240.

(25) Timoshkin, A. Y.; Bettinger, H. F.; Schaefer, H. F., III. *J. Phys. Chem. A* **2001**, *105*, 3249.

(26) Mihopoulos, T. Ph.D. Thesis, Massachusetts Institute of Technology, Cambridge, MA, 1999.

(27) Heuts, J. P. A.; Gilbert, R. G.; Radom, L. *J. Phys. Chem.* **1996**, *100*, 18997.

(28) Wolbank, B.; Schmid, R. *Chem. Vap. Deposition* **2003**, *9*, 272.

(29) Lorant, F.; Behar, F.; Goddard, W. A., III; Tang, Y. *J. Phys. Chem. A* **2001**, *105*, 7896.

(30) Frisch, M. J.; Trucks, G. W.; Schlegel, H. B.; Scuseria, G. E.; Robb, M. A.; Cheeseman, J. R.; Zakrzewski, V. G.; Montgomery, J. A., Jr.; Stratmann, R. E.; Burant, J. C.; Dapprich, S.; Millam, J. M.; Daniels, A. D.; Kudin, K. N.; Strain, M. C.; Farkas, O.; Tomasi, J.; Barone, V.; Cossi, M.; Cammi, R.; Mennucci, B.; Pomelli, C.; Adamo, C.; Clifford, S.; Ochterski, J.; Petersson, G. A.; Ayala, P. Y.; Cui, Q.; Morokuma, K.; Malick, D. K.; Rabuck, A. D.; Raghavachari, K.; Foresman, J. B.; Cioslowski, J.; Ortiz, J. V.; Stefanov, B. B.; Liu, G.; Liashenko, A.; Piskorz, P.; Komaromi, I.; Gomperts, R.; Martin, R. L.; Fox, D. J.; Keith, T.; Al-Laham, M. A.; Peng, C. Y.; Nanayakkara, A.; Gonzalez, C.; Challacombe, M.; Gill, P. M. W.; Johnson, B. G.; Chen, W.; Wong, M. W.; Andres, J. L.; Head-Gordon, M.; Replogle, E. S.; Pople, J. A. *Gaussian 98*, revision A.11.1; Gaussian, Inc.: Pittsburgh, PA, 2001.

(31) Becke, A. D. *J. Chem. Phys.* **1993**, *98*, 5648.

(32) Lee, C.; Yang, W.; Parr, R. G. *Phys. Rev. B: Condens. Matter Mater. Phys.* **1988**, *37*, 785.

(33) Wilson, A. K.; Woon, D. E.; Peterson, K. A.; Dunning, T. H. *J. Chem. Phys.* **1999**, *110*, 7667.

(34) Bauernschmitt, R.; Ahlrichs, R. *J. Chem. Phys.* **1996**, *104*, 9047.

(35) Boys, S. F.; Bernardi, F. *Mol. Phys.* **1970**, *19*, 553.

(36) Pelekh, A.; Carr, R. W. *J. Phys. Chem. A* **2001**, *105*, 4697.

(37) Trachtman, M.; Beebe, S.; Bock, C. W. *J. Phys. Chem.* **1995**, *99*, 15028.

(38) Bock, C. W.; Trachtman, M. *J. Phys. Chem.* **1994**, *98*, 95.

(39) Woon, D. E.; Dunning, T. H., Jr. *J. Chem. Phys.* **1994**, *101*, 8877.

(40) Woon, D. E.; Dunning, T. H., Jr. *J. Chem. Phys.* **1993**, *99*, 1914.

(41) Allendorf et al. claim an accuracy of ±8 kJ/mol (±2 kcal/mol) for their G2 calculated Ga−C bond energy in ref 12.

(42) We refer to the bottom of the well energy E_{elec}, since the zero-point energy is contained in the vibrational partition functions within q_{int}.

(43) Jensen, F. *Introduction to Computational Chemistry*; John Wiley & Sons: Weinheim, 1999.

(44) This form of the partition function includes the zero-point energy and is referenced to the "bottom of the well" energy E_{elec}.

(45) Truhlar, D. G. *J. Comput. Chem.* **1991**, *12*, 266.

(46) Schaftenaar, G. *MOLDEN*, CMBI: Nijmegen, 1999.

(47) Smith, D. *J. Chem. Phys.* **1980**, *73*, 3947.

(48) Sipachev, V. A. *J. Mol. Struct.* **1985**, *121*, 143.

(49) The maxima $\Delta G^{\ddagger}$ and $rc^{\ddagger}$ have been determined from the maximum of a quadratic fit to a set of three discrete datapoints, which were chosen to be the data point with the maximal ΔG and the two adjacent points.

(50) Schmid, R.; Cadenbach, T. Unpublished results.